Steady flow of smooth, inelastic particles on a bumpy inclined plane: Hard and soft particle simulations

Anurag Tripathi and D. V. Khakhar*

Department of Chemical Engineering, Indian Institute of Technology Bombay, Powai, Mumbai 400076, India

(Received 7 April 2009; revised manuscript received 19 November 2009; published 28 April 2010)

We study smooth, slightly inelastic particles flowing under gravity on a bumpy inclined plane using event-driven and discrete-element simulations. Shallow layers (ten particle diameters) are used to enable simulation using the event-driven method within reasonable computational times. Steady flows are obtained in a narrow range of angles ($13°-14.5°$); lower angles result in stopping of the flow and higher angles in continuous acceleration. The flow is relatively dense with the solid volume fraction, $\nu \approx 0.5$, and significant layering of particles is observed. We derive expressions for the stress, heat flux, and dissipation for the hard and soft particle models from first principles. The computed mean velocity, temperature, stress, dissipation, and heat flux profiles of hard particles are compared to soft particle results for different values of stiffness constant (k). The value of stiffness constant for which results for hard and soft particles are identical is found to be $k \geq 2 \times 10^6 mg/d$, where m is the mass of a particle, g is the acceleration due to gravity, and d is the particle diameter. We compare the simulation results to constitutive relations obtained from the kinetic theory of Jenkins and Richman [J. T. Jenkins and M. W. Richman, Arch. Ration. Mech. Anal. **87**, 355 (1985)] for pressure, dissipation, viscosity, and thermal conductivity. We find that all the quantities are very well predicted by kinetic theory for volume fractions $\nu < 0.5$. At higher densities, obtained for thicker layers ($H=15d$ and $H=20d$), the kinetic theory does not give accurate prediction. Deviations of the kinetic theory predictions from simulation results are relatively small for dissipation and heat flux and most significant deviations are observed for shear viscosity and pressure. The results indicate the range of applicability of soft particle simulations and kinetic theory for dense flows.

DOI: 10.1103/PhysRevE.81.041307 PACS number(s): 45.70.−n, 83.10.Rs, 47.45.Ab, 44.10.+i

I. INTRODUCTION

We consider a layer of particles flowing on an inclined surface under the influence of gravity, often referred to as a *chute flow*. The system is a configuration of practical relevance that preserves the fundamental complexity inherent to granular rheology and yet is simple enough for detailed analysis. The parameters of the system, in addition to particle properties, are the inclination of the surface (θ) and the height (h) of the flowing layer. Various experimental [1–4] and numerical [5–9] studies have been done to understand the flow behavior of granular materials in this geometry. Most of the numerical studies incorporate friction to mimic the real frictional grains and focus upon different issues such as the effect of particle properties [7,10], side wall effects [9,11,12], effect of layer thickness [6,13], boundary effects [14–17], flow initiation, and transition to jamming [18].

Individual particles may be modeled as either hard particles or as soft particles in numerical studies. Hard particle simulations are event driven (ED) and suffer from simulation artifact called *inelastic collapse* [19] in which the interval between collisions, for a sequence of collisions occurring between a pair of particles, goes to zero. The result is an infinite number of collisions in a finite time due to reduction of the relative normal velocity with each collision. Inelastic collapse occurs typically in high-density regimes of the flow. As a consequence, most of the studies of granular flow under gravity, in which high densities are typical, utilize discrete element (DE) simulations where the particles are modeled as deformable soft particles characterized by stiffness constant, k.

The materials typically used in experimental studies (such as glass, steel, etc.) have stiffness constants of the order of $k=10^9\ mg/d$ [20], where m is mass of the particle, d is the diameter of the particle, and g is the acceleration due to gravity. Simulating soft particles with these realistic values of the stiffness constants results in a computational step that is so small as to make large scale simulations infeasible. For computational convenience, the values of k used are typically 4 orders of magnitude smaller which correspond to those for soft rubber balls. Small values of k may cause an unphysically large duration of contacts giving rise to so-called "detachment effect" in DE simulations leading to erroneous results [10,21,22].

Thus it is important to know the soft particle stiffness beyond which the behavior approaches the infinitely stiff hard particle behavior in flows of practical importance. This limit is also required for comparison of granular kinetic theories [23,24], which assume the particles to be infinitely stiff. This issue has been considered previously for two-dimensional (2D) flows in chute flow [25] and homogeneous shear flow [26]. Mitarai and Nakanishi [25] observed in their 2D simulations of frictional disks that for large values of stiffness constant ($k \geq 2 \times 10^5\ mg/d$), the collision rate and the average multiple contact time fractions approach that for hard particle system only in the low-density limit ($\nu < 0.2$). For high densities ($\nu \sim 0.8$), even for particle stiffness as large as $k \sim 10^{10}\ mg/d$, soft particle behavior does not approach the hard particle behavior. However, microlevel inter-

*khakhar@iitb.ac.in

actions for three-dimensional (3D) simulations observed by Silbert *et al.* [27] and Reddy and Kumaran [28] reveal that for layers as thick as $H \sim 100d$ under chute flow, the contacts are predominantly hard-particle-like binary collisions for sufficiently stiff particles ($k \geq 2 \times 10^5 \ mg/d$) even near the base where the density is fairly high.

On a macroscopic scale, Ketterhagen *et al.* [26] compared the stresses under uniform 2D shear flow for hard and soft particles and found that for sufficiently stiff soft particles ($k \geq 7.85 \times 10^4 \rho d^2/\dot{\gamma}^2$), stresses are identical to those for hard particles. Reddy and Kumaran [28] found that Bagnold coefficients for chute flow of soft particles are almost identical to those obtained from shear flow of hard particles under similar density regimes. Recently, Klongboonjit and Campbell [29] showed that convection rolls observed in vertically vibrated beds disappear for very high values of stiffness constants for soft particles whereas hard particle simulations, which correspond to infinitely stiff particles, show the presence of convection rolls [30]. A detailed comparison of all flow parameters for hard and soft particles is lacking. Although the expression for calculation of stress tensor from simulation is well known for both particle models, a derivation from first principles has not been previously reported. The granular heat flux has either been obtained from an energy balance [31,32] or a constitutive relation [33] and a method of direct calculation from simulations is not available.

Kinetic theories for frictionless particles have been available for long [23,24,34] and kinetic theories for slightly frictional particles have also been developed [35–37]. However, there have been relatively few attempts to test the various constitutive equations obtained from kinetic theories of smooth particles in detail. Uniform [38–40] or boundary-driven [41–43] shear flow has been widely used for kinetic theory studies of smooth particles. Most of the studies have been done for 2D systems and only a few studies [38,39,41] have considered 3D granular flows.

Monte Carlo simulations of uniform shear flows give good agreement with kinetic theory predictions for a range of densities [39,40,44]. Numerical studies of uniform shear flows in high-density limits [38] have found deviations for normal stress and dissipation as predicted from kinetic theory and have been attributed to the presence of velocity correlations. Kinetic theory has also been able to predict velocity, density and stresses, [42] and particle flux [45] (2D) along with quite reasonable predictions of self-diffusion [41] (3D) for boundary driven flows.

Heated granular media [31,46–49] have been another popular choice for granular kinetic theory comparisons. However, properties such as thermal conductivity (κ) have been successfully predicted by kinetic theories either for very small inelasticities ($e=0.99$) [48] or for very small densities [49] ($\nu < 0.1$ for $e=0.92$). Dissipation and viscosity, however, have been relatively well predicted by the theory [31,47].

One objective of this work is to compare the results of hard and soft particle simulations for soft particles of different stiffness for a system of practical importance at relatively high solids fractions. We restrict our study to relatively shallow flows ($h \sim 10d$) to avoid inelastic collapse [50]. We consider an idealized system of smooth particles, which enables us to directly compare our numerical results to constitutive equations from kinetic theory for smooth, slightly inelastic particles in a dense flow. The focus here is on a detailed test of constitutive relations for pressure, stress, dissipation, heat flux, and self-diffusivity by comparison of numerical results to theoretical predictions. We also extend the study of kinetic theory constitutive equations to thicker layers and investigate the deviation of kinetic theory predictions for various quantities of interest including normal stress and dissipation rate at higher densities.

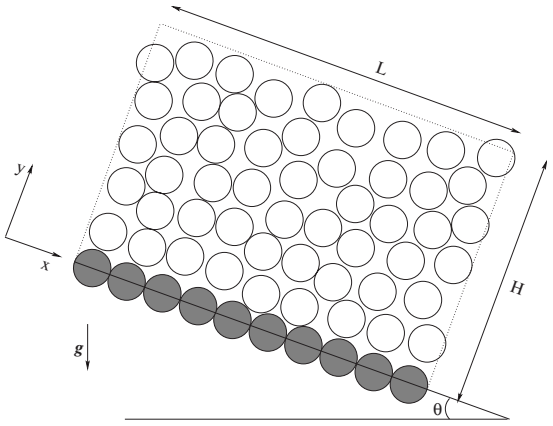

FIG. 1. 2D schematic of the chute flow configuration. x is the flow direction and z (out of the plane of paper) is the neutral direction. θ is the inclination angle and periodic simulation box is $10d \times 10d$ long and wide in x and z directions, respectively. Shaded spheres correspond to the particles fixed at the base.

The organization of the paper is as follows. Section II describes the hard and soft particle models and the simulation methodology for both event-driven and discrete-element simulations. Expressions for calculating stress tensor, dissipation, and granular heat flux vector are derived from first principles in Sec. III. Balance equations from continuum descriptions for the steady chute flow case along with kinetic theory constitutive equations are given in Sec. IV. Results and discussions are presented in Sec. V followed by conclusions.

II. SIMULATION METHODOLOGY

We simulate frictionless, slightly inelastic ($e=0.9$) monodisperse spheres of diameter d and mass m flowing on a bumpy inclined surface schematically depicted in Fig. 1. The simulation box is chosen to be $10d \times 10d$ long and wide in the x and z directions. The layer height in y direction is approximately $10d$. We use periodic boundary conditions in the x (flow) and z (neutral) directions so as to simulate an infinitely long and wide chute without end effects or sidewall effects. The chute base is made rough by sticking spheres of the same size as of the flowing particles and the base particles are arranged in a square lattice touching each other. At the start of the simulation, the flowing particles are arranged with their centers on a cubic lattice with side $1.1d$ so that no two particles are in contact. Particles are given random initial velocities. The chute angle, θ, is kept sufficiently high (θ

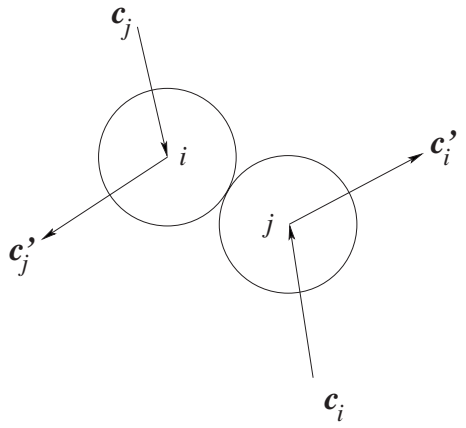

FIG. 2. Schematic of hard particle collision. $\boldsymbol{c}_i$, $\boldsymbol{c}_j$ are velocities just before the collision and $\boldsymbol{c}_i'$, $\boldsymbol{c}_i'$ are velocities just after the collision of particles i and j.

$=30°$) for an initial period so that particles accelerate and gain energy. The inclination is then reduced to a smaller value and the flow is allowed to achieve steady state, if one exists. Individual particles are modeled either as nondeformable hard particles or as deformable soft particles as described below.

A. Hard particle model

Particles in this model are considered infinitely stiff and hence the collision time is zero. As a result, only one collision or "event" is allowed at a given instant. This also implies that only binary collisions are permitted and multiparticle contacts cannot be accounted for.

The particles move freely under the influence of gravity until a collision occurs. From the positions and velocities of particles, the pair of particles colliding next is identified and the duration (Δt) after which the collision to occur is calculated as described below. All the particles are then moved for time Δt using the equations of motion. Since the particles are frictionless, the tangential component of the velocities of the colliding particles remains unchanged after the collision. Considering momentum conservation and the definition of normal restitution coefficient, the post-collision velocities of colliding particles i and j are easily calculated and are given by the collision rule in Ref. [23] for the case when both the particles are moving. The post-collision velocity $\boldsymbol{c}_i'$ of a moving particle i colliding with a static boundary particle j is given by

$$\boldsymbol{c}_i' = \boldsymbol{c}_i - (1+e)(\boldsymbol{n}_{ij}\cdot\boldsymbol{c}_i)\boldsymbol{n}_{ij}, \tag{1}$$

where $\boldsymbol{n}_{ij}=(\boldsymbol{x}_i-\boldsymbol{x}_j)/|\boldsymbol{x}_i-\boldsymbol{x}_j|$ and $\boldsymbol{x}_i$ and $\boldsymbol{c}_i$ are position and velocity of particle i, respectively (see Fig. 2). The velocities of the colliding particles are then updated. The above steps of calculating the time interval (Δt) for the next collision, moving all particles for Δt and updating the velocities of the colliding pair, are repeated.

The procedure used to calculate the duration for the next collision is as follows. The time interval for collision (Δt_{ij}) for every probable pair of particles is calculated. The time interval for the next collision (Δt) corresponds to the pair with the minimum positive Δt_{ij}. The condition for collision between a pair of particles i,j is

$$|\boldsymbol{x}_i(t+\Delta t)-\boldsymbol{x}_j(t+\Delta t)| = d. \tag{2}$$

For the case when both particles are moving, Δt is calculated by solving the quadratic equation

$$a\Delta t^2 + b\Delta t + c = 0, \tag{3}$$

where coefficients are defined as $a=\boldsymbol{c}_{ij}\cdot\boldsymbol{c}_{ij}$, $b=2\boldsymbol{c}_{ij}\cdot\boldsymbol{x}_{ij}$, and $c=\boldsymbol{x}_{ij}\cdot\boldsymbol{x}_{ij}-d^2$, with $\boldsymbol{x}_{ij}=\boldsymbol{x}_i-\boldsymbol{x}_j$. For a moving particle colliding with a static bottom particle, we obtain a quartic equation

$$a\Delta t^4 + b\Delta t^3 + c\Delta t^2 + d\Delta t + e = 0, \tag{4}$$

where $a=(\boldsymbol{g}\cdot\boldsymbol{g})/4$, $b=\boldsymbol{g}\cdot\boldsymbol{c}_i$, $c=\boldsymbol{c}_i\cdot\boldsymbol{c}_i+\boldsymbol{g}\cdot\boldsymbol{x}_{ij}$, $d=2\boldsymbol{c}_i\cdot\boldsymbol{x}_{ij}$, and $e=\boldsymbol{x}_{ij}\cdot\boldsymbol{x}_{ij}-d^2$. $\boldsymbol{x}_i$ and $\boldsymbol{c}_i$ are the position and velocity of moving particle i colliding with static particle j at $\boldsymbol{x}_j$. To obtain Δt, we solve Eq. (4) using Ferarri's method for general quartic equations [51,52].

Several methods have been proposed to avoid *inelastic collapse* [53–55], a simulation artifact that has restricted the applicability of hard particle simulations to relatively dilute flows. We use the model proposed by Luding and McNamara [19] in which a collision is assumed to be elastic ($e=1$) if a pair suffers a second collision within a time span that is less than a specified interval, t_c. We refer to this model as the TC model because of the finite time of collision incorporated in it. Incorporating the TC model switches off the dissipation whenever such a situation arises and hence Δt does not reduce beyond a minimum critical value and the simulation proceeds in very small steps until one of the particles in the trapped particle pair collides with another particle. However, for the TC model to remain valid, the number of forced zero-dissipation collisions must be a very small fraction of total number of collisions to ensure that the net energy in the system does not increase significantly.

B. Soft particle model

In the soft particle model, particles interact with each other for a finite time and deform during the interaction. The simulation advances by time steps small enough to capture each collision in several fine steps. The contact forces between interacting particles are usually assumed to depend on the deformation and rate of deformation. We employ a linear spring and dash-pot-type force scheme in our simulations. Since the particles are smooth, tangential forces are zero. Thus our force scheme is equivalent to the $L3$ model used in Ref. [7] with $e=0.9$ and $\mu=k_t=\gamma_t=0$.

The normal force, $\boldsymbol{F}_{ij}$, acting on particle i due to particle j is a summation of two parts: an elastic spring force that tends to push the particles apart and a viscous force that accounts for the dissipation during the interaction and is given by

$$\boldsymbol{F}_{ij} = k\alpha\boldsymbol{n}_{ij} - \gamma m_{eff}\boldsymbol{c}_{nij}, \tag{5}$$

where k is the stiffness and γ is the damping constant. In the above equation, $\alpha=(d-x_{ij})$ is the deformation with $x_{ij}=|\boldsymbol{x}_i-\boldsymbol{x}_j|$, $\boldsymbol{c}_{nij}=(\boldsymbol{n}_{ij}\cdot\boldsymbol{c}_{ij})\boldsymbol{n}_{ij}$ is the relative normal velocity, and $m_{eff}=m_im_j/(m_i+m_j)$ is the effective mass of the spheres with

masses m_i and m_j. For the case when both particles i and j are moving, $m_{eff}=m/2$ and for the interaction with base particle, assumed to be of infinite mass, $m_{eff}=m$. The force on particle j due to particle i is $\boldsymbol{F}_{ji}=-\boldsymbol{F}_{ij}$. Since the mass of base particles is infinite, the base particles do not move despite finite forces on them. The motion of any particle i under the influence of gravity ($\boldsymbol{g}$) and the force exerted by all other j particles is given by

$$\frac{d\boldsymbol{x}_i}{dt}=\boldsymbol{c}_i, \tag{6}$$

$$m\frac{d\boldsymbol{c}_i}{dt}=m\boldsymbol{g}+\sum_j \boldsymbol{F}_{ij}. \tag{7}$$

The above differential equations are integrated using second-order Runge-Kutta method with step size correction [56].

The choice of basic step size, dt, depends upon the stiffness, k. We use a base integration time step $dt=t_{col}/70$, where t_{col} is the contact duration of a binary collision given by [7]

$$t_{col}=\pi\left(\frac{2k}{m}-\frac{\gamma^2}{4}\right)^{-1/2} \tag{8}$$

for identical particles with mass m, for a binary collision of soft particles with the linear spring dash-pot force scheme. The normal restitution coefficient for this case is given by

$$e=\exp\left(\frac{-\gamma t_{col}}{2}\right). \tag{9}$$

Rearrangement of Eq. (9) using Eq. (8) gives

$$\gamma=\sqrt{\frac{8k(\ln e)^2}{m[\pi^2+(\ln e)^2]}}. \tag{10}$$

Thus for a specified value of the coefficient of restitution, e, Eq. (10) is used to calculate γ for the different values of stiffness.

III. CALCULATION OF STRESS AND HEAT FLUX

The stress and the heat flux, i.e., the flux of fluctuation kinetic energy, have contributions from two distinct mechanisms: streaming (due to velocity fluctuations) and contact between particles. The expressions for the streaming component (which are the same for hard and soft particles) are widely reported and are given in the next section for the sake of completeness. This is followed by expressions for contact stress, and dissipation and heat flux for hard and soft particles, respectively. Although Campbell and Gong [57] gave expressions for the stress tensor for hard particle model, we present here derivation for the stress tensor due to collisions for hard particles along with the derivation of heat flux. We also derive expressions for the stress tensor, dissipation, and heat flux due to contacts for soft particles from first principles in this section. Expressions for heat flux and dissipation have not been previously reported.

A. Streaming components

The streaming stress is defined as the rate of transfer of momentum per unit area due to velocity fluctuations and is given by [58]

$$\boldsymbol{\sigma}^s=\frac{1}{V}\sum_{i=1}^{N} m\boldsymbol{C}_i\boldsymbol{C}_i=\rho\langle\boldsymbol{C}_i\boldsymbol{C}_i\rangle, \tag{11}$$

where $\boldsymbol{C}_i=\boldsymbol{c}_i-\boldsymbol{v}$ is the fluctuation velocity of particle i, $\boldsymbol{c}_i$ is the instantaneous velocity of the particle i, $\boldsymbol{v}=\langle\boldsymbol{c}_i\rangle$ is the local number average velocity, and the average is over the N particles in a volume V. In the above equation $\rho=mN/V$, and the number average is defined as

$$\langle\odot\rangle=\frac{1}{N}\sum_{i=1}^{N}\odot. \tag{12}$$

On simplification, we obtain the streaming stress to be

$$\boldsymbol{\sigma}^s=\rho(\langle\boldsymbol{c}_i\boldsymbol{c}_i\rangle-\boldsymbol{v}\boldsymbol{v}). \tag{13}$$

The streaming heat flux ($\boldsymbol{q}^s$) is defined as the transport of fluctuation kinetic energy ($\frac{1}{2}m\boldsymbol{C}_i\cdot\boldsymbol{C}_i$) by velocity fluctuations and is given by

$$\boldsymbol{q}^s=\frac{1}{V}\sum_{i=1}^{N}\left(\frac{1}{2}m\boldsymbol{C}_i\cdot\boldsymbol{C}_i\right)\boldsymbol{C}_i. \tag{14}$$

Using the definition of fluctuation velocity and simplifying, the streaming heat flux is found to be

$$\boldsymbol{q}^s=\frac{1}{2}\rho\langle c_i^2\boldsymbol{c}_i\rangle-\boldsymbol{\sigma}^s\cdot\boldsymbol{v}-\left(\frac{1}{2}\mathrm{tr}(\boldsymbol{\sigma}^s)+\frac{1}{2}\rho v^2\right)\boldsymbol{v}. \tag{15}$$

B. Contact components

Consider a cuboid of volume $V(L_x\times L_y\times L_z)$ containing N contacting pair of particles. Since the mode of contact depends on the choice of the particle model, we derive expressions for hard and soft particle models separately, starting with the hard particle case.

1. Hard particle model

We calculate stress for hard particle system as the net rate of transfer of momentum due to collisions across a surface with a unit normal $\boldsymbol{n}$ as shown in Fig. 3. A collision results in a net transfer of momentum across the surface only if the centers of the colliding particles lie on either side of the plane. The momentum gained by particle i due to the collision is

$$\Delta\boldsymbol{P}_{ij}=m(\boldsymbol{c}_i'-\boldsymbol{c}_i)=-m(\boldsymbol{c}_j'-\boldsymbol{c}_j) \tag{16}$$

and corresponds to the momentum transfer by the collision. The probability of the colliding particles' centers lying on either side of the surface is

$$\wp_{ij}=\frac{|\boldsymbol{x}_{ij}\cdot\boldsymbol{n}|}{L_y}. \tag{17}$$

The stress vector ($\boldsymbol{T}$) defined as the rate of transfer of momentum per unit area across the surface is then

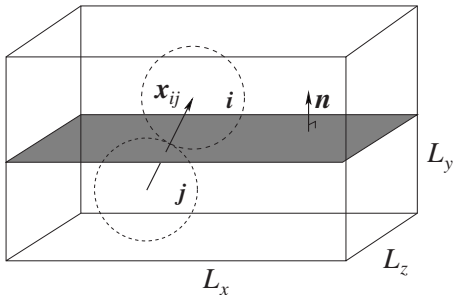

FIG. 3. Pair of contacting particles in volume V. The unit normal to the shaded surface is denoted as $\boldsymbol{n}$ and $\boldsymbol{x}_{ij}$ is the vector joining the centers of particles.

$$\boldsymbol{T} = \frac{1}{L_x L_z \delta t} \sum_{N_c} \Delta \boldsymbol{P}_{ij} \wp_{ij}, \tag{18}$$

where δt is the time duration in which N_c collisions occur. By definition, the stress tensor ($\boldsymbol{\sigma}$) is related to the stress vector as $\boldsymbol{T}=\boldsymbol{\sigma}\cdot\boldsymbol{n}$. Thus the collision stress tensor is

$$\boldsymbol{\sigma}^c = \frac{1}{V \delta t} \sum_{N_c} m(\boldsymbol{c}_i' - \boldsymbol{c}_i)\boldsymbol{x}_{ij}. \tag{19}$$

We have removed the modulus sign since interchanging particles i and j do not make any difference to the expression because of momentum conservation in a collision [Eq. (16)]. Further, in the absence of friction, there are no couple forces and the stress tensor is symmetric.

Consider next the heat flux across the surface, defined as the net rate of transfer of fluctuation kinetic energy due to collisions across the surface with unit normal $\boldsymbol{n}$. A collision between two inelastic particles results in loss of part of the kinetic energy of one of the particles. A part of this loss is dissipated and the rest is transferred to other particle, so that

$$\Delta K^- = \Delta K^+ + \varepsilon, \tag{20}$$

where ε is the energy dissipated in the collision and ΔK^- and ΔK^+ are the loss and gain in fluctuation kinetic energy of the respective particles due to the collision. Assume that particle i gains energy after the collision so that

$$\Delta K^+ = \frac{1}{2} m(|\boldsymbol{c}_i' - \boldsymbol{v}|^2 - |\boldsymbol{c}_i - \boldsymbol{v}|^2). \tag{21}$$

Taking into account the direction of the transfer, the energy transferred across the surface because of the collision is

$$\Delta E = \Delta K^+ \frac{\boldsymbol{x}_{ij}\cdot\boldsymbol{n}}{|\boldsymbol{x}_{ij}\cdot\boldsymbol{n}|}. \tag{22}$$

Considering the probability of collisions which span the surface [Eq. (17)], the energy transfer per unit area per unit time is

$$q_n^c = \frac{1}{L_x L_z \delta t} \sum_{N_c} \Delta E \wp_{ij}. \tag{23}$$

On simplification and using $q_n^c = \boldsymbol{q}^c\cdot\boldsymbol{n}$, we get the expression for the heat flux vector due to collisions as

$$\boldsymbol{q}^c = \frac{1}{V \delta t} \sum_{N_c} \Delta K^+ \boldsymbol{x}_{ij}. \tag{24}$$

The dissipation rate (Γ), defined as energy loss per unit volume per unit time due to inelastic collisions, is obtained by considering sum of the change of kinetic energy of each colliding pair over time interval δt as

$$\Gamma = \frac{1}{V \delta t} \sum_{N_c} \varepsilon, \tag{25}$$

which upon simplification yields

$$\Gamma = \frac{m}{2V \delta t} \sum_{N_c} (c_i^2 + c_j^2) - (c_i'^2 + c_j'^2). \tag{26}$$

2. Soft particle model

Consider next the contact stress for the soft particle model. The stress on the surface with normal vector $\boldsymbol{n}$ is due to forces exerted by particle pairs in contact with each other with their centers lying on either side of the surface. The force on the surface is

$$\boldsymbol{F}_{tot} = \sum_{N_c} \boldsymbol{F}_{ij} \wp_{ij}, \tag{27}$$

where $\wp_{ij}$ [Eq. (17)] is the probability of the contacting pair being on either side of the surface and the summation is over all N_c contacts in volume V. The stress acting on the surface with unit normal $\boldsymbol{n}$ is then

$$\boldsymbol{\sigma}^c \cdot \boldsymbol{n} = \frac{\boldsymbol{F}_{tot}}{L_x L_z} = \sum_{N_c} \frac{\boldsymbol{F}_{ij}\boldsymbol{x}_{ij}\cdot\boldsymbol{n}}{L_x L_y L_z}. \tag{28}$$

Hence, contact stress tensor $\boldsymbol{\sigma}^c$ is

$$\boldsymbol{\sigma}^c = \frac{1}{V} \sum_{N_c} \boldsymbol{F}_{ij}\boldsymbol{x}_{ij}. \tag{29}$$

As found above for hard particles, the stress tensor is symmetric. Using the same construction as above, we calculate the contact heat flux for soft particles as the net rate of work done by contact forces due to velocity fluctuations. The net rate of work done is

$$W_{ij} = \boldsymbol{F}_{ij}\cdot(\boldsymbol{c}_m - \boldsymbol{v}), \tag{30}$$

where $\boldsymbol{c}_m = (\boldsymbol{c}_i + \boldsymbol{c}_j)/2$ is the velocity of the contact point. The rate of energy transfer per unit area across the surface is then

$$q_n^c = \frac{1}{L_x L_z} \sum_{N_c} W_{ij} \wp_{ij}. \tag{31}$$

On simplifying as above, we obtain the contact heat flux vector as

$$\boldsymbol{q}^c = \frac{1}{V} \sum_{N_c} \boldsymbol{F}_{ij}\cdot\boldsymbol{c}_m \boldsymbol{x}_{ij} - \boldsymbol{v}\cdot\boldsymbol{\sigma}^c. \tag{32}$$

Note that final expressions for stress and heat flux remain unchanged when i and j are interchanged in the expression and hence removing the modulus sign for $\wp_{ij}$ in Eq. (17) does not make any difference.

TABLE I. Normalization of various quantities of interest.

Dimensionless quantity	Scaling	Dimensionless quantity	Scaling
$\bar{\boldsymbol{x}}$	$\frac{\boldsymbol{x}}{d}$	$\bar{\boldsymbol{\sigma}}$	$\frac{\boldsymbol{\sigma}}{mg/d^2}$
$\bar{V}$	$\frac{V}{d^3}$	$\bar{P}$	$\frac{P}{mg/d^2}$
$\bar{n}$	nd^3	$\bar{\boldsymbol{\tau}}$	$\frac{\boldsymbol{\tau}}{mg/d^2}$
$\bar{t}$	$\frac{t}{\sqrt{d/g}}$	$\bar{E}$	$\frac{E}{mgd}$
$\bar{\alpha}$	$\frac{\alpha}{d}$	$\bar{\gamma}$	$\frac{\gamma}{\sqrt{g/d}}$
$\bar{\boldsymbol{v}}$	$\frac{\boldsymbol{v}}{\sqrt{gd}}$	$\bar{\Gamma}$	$\frac{\Gamma}{mg^{3/2}/d^{5/2}}$
$\bar{T}$	$\frac{T}{gd}$	$\bar{k}$	$\frac{k}{mg/d}$
$\bar{\boldsymbol{F}}$	$\frac{\boldsymbol{F}}{mg}$	$\bar{\boldsymbol{q}}$	$\frac{\boldsymbol{q}}{mg^{3/2}/d^{3/2}}$

The dissipation rate for the soft particle case is obtained as the rate of work done per unit volume by the damping force due to the relative motion of particles and is given by

$$\Gamma = \sum_{N_c} \frac{\boldsymbol{F}_d \cdot \boldsymbol{c}_{ij}}{V}, \tag{33}$$

where $\boldsymbol{F}_d = \gamma m_{eff} \boldsymbol{c}_{nij}$. On simplification, we get

$$\Gamma = \sum_{N_c} \frac{\gamma m_{eff} c_{nij}^2}{V}. \tag{34}$$

C. Dimensionless expressions

We nondimensionalize all the quantities of interest and represent dimensionless quantities with an overbar. The definitions of all dimensionless quantities are given in Table I. Using these definitions, dimensionless expressions for stress, heat flux, and dissipation rate are given below.

The streaming component of stress tensor is given as

$$\bar{\boldsymbol{\sigma}}^s = \bar{n}(\langle \bar{\boldsymbol{c}}_i \bar{\boldsymbol{c}}_i \rangle - \bar{\boldsymbol{v}}\bar{\boldsymbol{v}}),$$

where $\bar{n} = N/\bar{V}$. The collisional component of the stress tensor is

$$\bar{\boldsymbol{\sigma}}^c = \begin{cases} \frac{1}{\bar{V}\bar{\delta t}} \sum_{N_c} (\bar{\boldsymbol{c}}_i' - \bar{\boldsymbol{c}}_i)\bar{\boldsymbol{x}}_{ij}, & \text{hard particle} \\ \frac{1}{\bar{V}} \sum_{N_c} \bar{\boldsymbol{F}}_{ij}\bar{\boldsymbol{x}}_{ij}, & \text{soft particle,} \end{cases}$$

where $\bar{\boldsymbol{F}}_{ij} = \bar{k}\bar{\alpha}\hat{\boldsymbol{n}}_{ij} - \bar{\gamma} m_{eff} \bar{\boldsymbol{c}}_{nij}/m$ and $\bar{\alpha} = (1 - \bar{x}_{ij})$. The total stress is then given by

$$\bar{\boldsymbol{\sigma}} = \bar{\boldsymbol{\sigma}}^s + \bar{\boldsymbol{\sigma}}^c.$$

Taking a hydrodynamic approach, the total stress may be written as $\bar{\boldsymbol{\sigma}} = -\bar{P}\mathbf{I} - \bar{\boldsymbol{\tau}}$, where $\bar{P} = \frac{1}{3}\mathrm{tr}(\bar{\boldsymbol{\sigma}})$ is the pressure and $\bar{\boldsymbol{\tau}}$ is the deviatoric stress. The total heat flux is

$$\bar{\boldsymbol{q}} = \bar{\boldsymbol{q}}^s + \bar{\boldsymbol{q}}^c,$$

where the streaming component of the heat flux vector is

$$\bar{\boldsymbol{q}}^s = \frac{1}{2}\bar{n}\langle \bar{c}_i^2 \bar{\boldsymbol{c}}_i \rangle - \bar{\boldsymbol{\sigma}}^s \cdot \bar{\boldsymbol{v}} - \left[\frac{1}{2}\mathrm{tr}(\bar{\boldsymbol{\sigma}}^s) + \frac{1}{2}\bar{n}\bar{v}^2 \right] \bar{\boldsymbol{v}}$$

and the contact component is

$$\bar{\boldsymbol{q}}^c = \begin{cases} \frac{1}{\bar{V}\bar{\delta t}} \sum_{N_c} \Delta \bar{K}^+ \Delta \bar{\boldsymbol{x}}_{ij}, & \text{hard particle} \\ \frac{1}{\bar{V}} \sum_{N_c} \bar{\boldsymbol{F}}_{ij} \cdot \bar{\boldsymbol{c}}_m \bar{\boldsymbol{x}}_{ij} - \bar{\boldsymbol{v}} \cdot \bar{\boldsymbol{\sigma}}^c, & \text{soft particle.} \end{cases}$$

The expression for dissipation rate is

$$\bar{\Gamma} = \begin{cases} \frac{1}{2\bar{V}\bar{\delta t}} \sum_{N_c} (\bar{c}_i^2 + \bar{c}_j^2) - (\bar{c}_i'^2 + \bar{c}_j'^2), & \text{hard particle} \\ \sum_{N_c} \frac{m_{eff}\bar{\gamma}\bar{c}_{nij}^2}{m\bar{V}}, & \text{soft particle.} \end{cases}$$

IV. THEORY

We apply the granular kinetic theory for smooth, slightly inelastic spheres of Jenkins and Richman [34] to the case of steady, fully developed chute flow. We compare predictions of the theory to results of numerical simulations in two ways. (1) We compare the predictions of the integrated momentum and energy balance equations without the use of constitutive equations to numerical results for the shear stress, pressure, and heat flux. This is a consistency check of the numerical simulations and is used to show that the simulations satisfy the continuum momentum and energy balance equations. (2) We compare the predictions of theory for viscosity, thermal conductivity, and rate of dissipation due to inelastic collisions to numerical simulation results.

The governing equations simplified for the case under the study are

$$\frac{dv_x}{dx} = 0, \tag{35}$$

$$0 = -\frac{d\tau_{yx}}{dy} + \rho g \sin\theta, \tag{36}$$

$$0 = -\frac{dP}{dy} - \rho g \cos\theta, \tag{37}$$

$$0 = -\frac{dq_y}{dy} - \tau_{xy}\frac{dv_x}{dy} - \Gamma. \tag{38}$$

The continuity equation [Eq. (35)] is identically satisfied. Integrating the x and y momentum balance equations [Eq. (36) and (37)], we obtain

$$\tau_{xy} = -\int_y^\infty \rho g \sin\theta dy, \tag{39}$$

$$P = \int_y^\infty \rho g \cos\theta dy, \tag{40}$$

assuming $\tau_{xy}=P=0$ at $y=\infty$. Similarly, integration of the energy balance equation [Eq. (38)], assuming $q_y=0$ at $y=\infty$, gives

$$q_y = -\int_y^\infty \left[-\tau_{xy}\frac{dv_x}{dy} - \Gamma\right] dy. \tag{41}$$

We list next the constitutive relations obtained by Jenkins and Richman [34]. The equation of state for the pressure is given by

$$P = \rho(1+4G)T, \tag{42}$$

where $G=\nu(1-\nu/2)/(1-\nu)^3$ and $\nu=n\pi d^3/6$ is the solids volume fraction. The stress constitutive equation for the present case simplifies to

$$\tau_{xy} = -\mu\frac{dv_x}{dy} \tag{43}$$

and the viscosity is given by

$$\mu = (8J/5\pi^{1/2})\rho d G T^{1/2}, \tag{44}$$

with $J=1+(\pi/12)[1+5/(8G)]^2$. The heat flux is

$$q_y = -\kappa\frac{dT}{dy}, \tag{45}$$

with the thermal conductivity given by

$$\kappa = (4M/\pi^{1/2})\rho d G T^{1/2}, \tag{46}$$

where $M=1+(9\pi/32)[1+5/(12G)]^2$. Finally, the rate of dissipation due to inelastic collisions is given by

$$\Gamma = \frac{24}{\pi^{1/2}}\frac{\rho G}{d}(1-e)T^{3/2}. \tag{47}$$

Self-diffusivity, D, for inelastic spheres using concepts from dense-gas kinetic theory analysis has been calculated by various researchers [41,59–62] and the expression can be captured in the general form

$$D = \frac{d(\pi T)^{1/2}}{aG}, \tag{48}$$

with a being a constant. References [41,59,60] use $a=8(1+e)$, where as Ref. [62] use $a=16$. Using the expression given in Ref. [61] for the present case of equal-size and equal-mass particles, we obtain $a=4\sqrt{6}$.

V. RESULTS AND DISCUSSION

All the results presented here are in terms of dimensionless quantities and we drop the overbar notation for ease of representation.

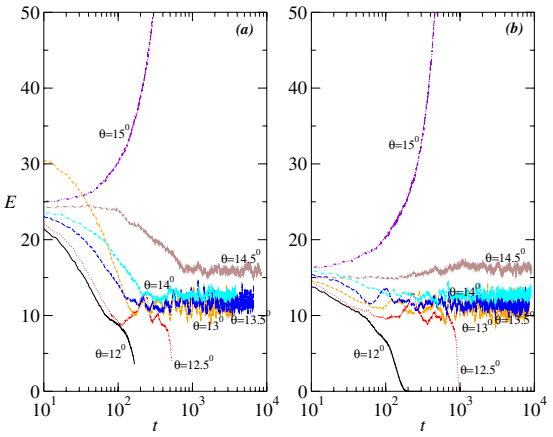

FIG. 4. (Color online) Average kinetic energy per particle with time at different inclinations for (a) hard and (b) soft particles ($k=2\times10^6$). Steady flow is possible only for $\theta\in[13°-14.5°]$. For $\theta=12°$ and 12.5° (bottom two lines), soft particle assembly comes to rest but the kinetic energy in case of hard particles does not go to zero due to advent of inelastic collapse despite using TC model.

A. Approach to steady state

We consider the approach of the system to steady state in terms of the variation of the average kinetic energy per particle with time. Figure 4 shows the typical behavior of the mean kinetic energy per particle for different inclination angles for hard particles and for soft particles with sufficiently high stiffness constant $k=2\times10^6$ mg/d. For small inclinations ($\theta\leq12.5°$), the granular layer comes to a rest and for high inclinations ($\theta=15°$), the particles accelerate. In the range of $\theta=13°-14.5°$, the work done by gravity is balanced by dissipation and a steady flow is achieved. Note that the fluctuation of kinetic energy about the mean value increases with decrease in θ, i.e., fluctuations grow as we approach jamming. The static limit does not exist for hard particle model and the assembly of hard particles does not come to rest as in case of the soft particle model. However, as shown in Fig. 4(a), the kinetic energy of hard particles decreases significantly (to almost 1/5th of steady-state value) for small inclinations ($\theta=12°$ and 12.5°). The average time between collisions keeps decreasing with time and a very large number of collisions occurs in a very small time as the hard particle system approaches the static limit.

Soft particles with stiffness $k\leq2\times10^4$ did not achieve steady state and accelerated in an unbounded manner at $\theta=14.5°$. Although a steady-state flow is achieved for $k=2\times10^5$, the steady-state kinetic energy is higher than the hard particle case. Particles with $k\geq2\times10^6$ have a kinetic energy identical to the hard particle system at steady state. The effect of t_c variation was found to be small provided t_c values used were sufficiently small as compared to average time interval between collisions, which is of the order of 10^{-2} for the hard particle simulation. For $t_c=10^{-2}$ and 10^{-3}, hard particles accelerate in an unbounded fashion and a significant portion of total number of collisions (about 30% for $t_c=10^{-2}$ and about 5% for $t_c=10^{-3}$) is forced to be nondissipative by TC model for these values of t_c. For smaller values of t_c, a steady state is obtained with a very small fraction (about

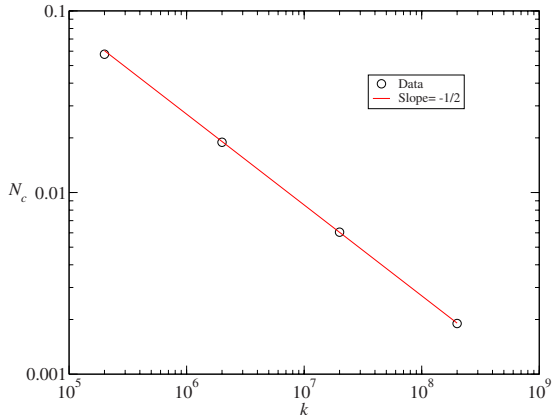

FIG. 5. (Color online) Average number of contacts per unit volume at any instant for soft particles of different stiffness. The fitted line is straight line with slope=−1/2.

2% for $t_c=10^{-4}$ and about 0.5% for $t_c=10^{-5}$) of total collisions being nondissipative. We use $t_c=10^{-5}$ in our hard particle simulations. This value of t_c corresponds to binary contact duration (t_{col}) for soft particles with $k\sim 10^9$.

B. Number of contacts

To gain a microscopic picture of grain interactions in case of soft particles, we take snapshots of the flow at intervals of t_{col} and plot average number of contacts (N_c) between particles per unit volume for different values of k. Figure 5 shows that average number of contacts decreases linearly with k on a log-log plot. The straight line in Fig. 5 has a slope of $-1/2$ giving $N_c \propto k^{-1/2}$. This can be understood as follows. For sufficiently stiff particles, all profiles, including dissipation rate profile, should be independent of k. This is in fact the case, as shown later in Fig. 9. Using Eq. (47), the dissipation rate (Γ) can be rewritten as $\Gamma = m\langle c_{nij}^2\rangle N_c \gamma / 2V$. For Γ and c_{nij}^2 to be independent of k, we must have $N_c \propto 1/\gamma$. Since $\gamma \propto k^{1/2}$ [Eq. (10)], we get $N_c \propto k^{-1/2}$ in agreement with the numerical results.

C. Comparison of hard and soft particle results

We compare the results for the hard particle model to the soft particle model for different values of particle stiffness, k, in this section. The simulation cell is divided in strips of width $0.1d$ along y direction. Results are obtained by measuring the relevant quantities in each strip at steady state for 100 dimensionless time units and are averaged over five such consecutive sets. We plot every third data point for clarity. Since the range of steady flow is narrow and fluctuations are significant for lower values of steady-state inclination, we compare all our results at $\theta=14.5°$ for hard and soft particles. Figures 6–11 show the simulation results of soft particles for three different values of k and for hard particles.

Figure 6 shows the mean velocity profiles for the flow. The velocity is maximum near the free surface with very small slip near the base. The error bars in all cases are small except near the free surface where the number density is very low. The velocity profile for $k=2\times 10^5$ (red squares) deviates

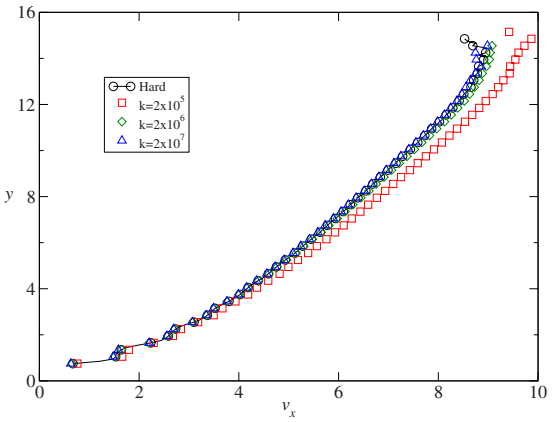

FIG. 6. (Color online) Velocity profiles for hard and soft particle (with different stiffness constants) simulations. Error bars are shown only for hard particle velocity profile for the sake of clarity. Maximum velocity for $k=2\times 10^5$ (red squares) is ≈10% higher than the maximum velocity for hard particles (black circles).

significantly from the hard particle (black circles) case and the maximum velocity is 10% higher than the hard particle case. However, the profiles for the soft particle case for $k \geq 2\times 10^6$ (green diamonds and blue triangles) are identical to those for the hard particle case.

Figure 7 shows the granular temperature profile. The temperature is highest at the base and decreases to a nearly constant low value near the free surface. The results are reasonable considering that the viscous dissipation ($\tau_{xy} dv_x/dy$) is highest at the base and approaches zero near the free surface. Again, the profile for soft particles with $k=2\times 10^5$ (red squares) deviates significantly from the hard particle (black circle) case but the soft particle profiles are identical to the hard particle profiles for $k\geq 2\times 10^6$. The temperature for $k=2\times 10^5$ is higher than the hard particle case. Figure 8(a) gives the number density profile, which shows sharp peaks, indicating layering of particles. The solids volume profile [Fig. 8(b)] does not show peaks since a larger averaging volume (bin height $1d$) is taken. The volume fraction of solids gradually increases with depth from the free surface and reaches a maximum value of $\nu \approx 0.5$ instead of being con-

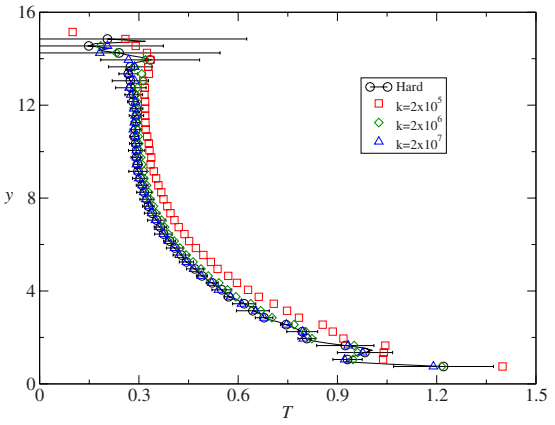

FIG. 7. (Color online) Granular temperature profile for hard and soft particle models. Discrepancy for soft particles with $k=2\times 10^5$ (squares) is evident.

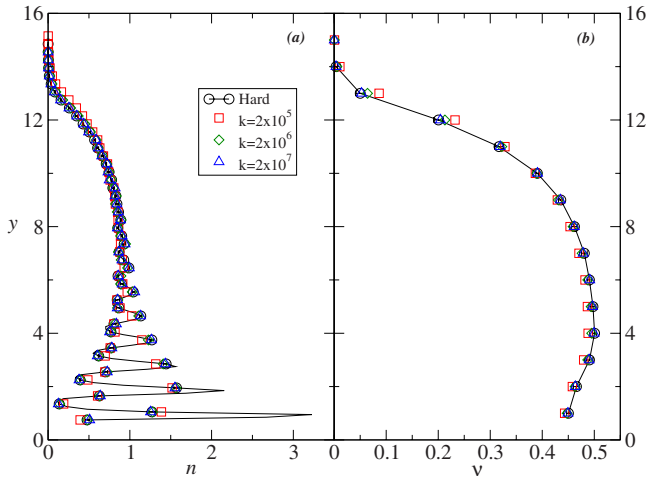

FIG. 8. (Color online) (a) Number density and (b) solids fraction profile for hard and soft particle models. Strip size for number density profile is $0.1d$ whereas solids fraction profiles are obtained using strip size$=1d$.

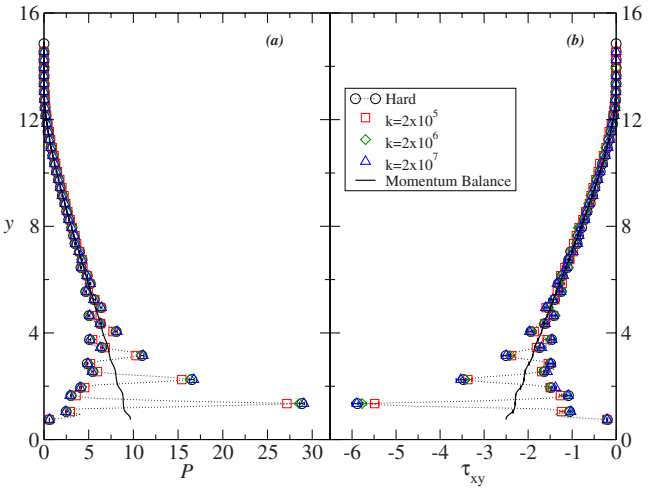

FIG. 10. (Color online) (a) Normal stress and (b) shear stress profile from hard and soft particle models. Solid line represents the momentum balance estimate of the stresses from Eqs. (39) and (40).

stant through out the layer. This is because a necessary condition for constant density across the layer is that the heat flux be negligible, which is the case for frictional particles, but not for smooth particles as can be seen in Fig. 11. There is a slight decrease near the base due to the high temperatures. The soft particle profiles with the lowest stiffness, i.e., $k=2\times10^5$ (red squares) deviate only slightly near the free surface from the hard particle case.

Figure 9 shows the profile for the dissipation due to inelastic collisions. The dissipation is highest near the base and decreases monotonically with height. This is because dissipation depends on the number density and temperature and both decrease monotonically with height in the layer. Figure 10 shows the pressure (P) and shear stress (τ_{xy}) profiles. Both vanish near the free surface and increase nearly linearly with depth. The latter is a consequence of a nearly constant bulk density in the flowing layer. Finally, Fig. 11 shows the heat flux (q_y) profiles in which q_y is maximum at the base and goes to zero at the free surface. This is because the temperature gradient is maximum near the base and nearly zero at the free surface. In all the profiles shown in Figs. 9–11, the profiles for the soft particles and hard particles are nearly identical.

Results obtained from soft particle simulations for $k=2\times10^5$ are significantly different from the hard particle results. However, the hard and soft particle results match for $k\geq2\times10^6$ for a layer of about ten particles deep. We note that the value of stiffness reported in previous studies beyond which the effect of stiffness is small is $k=2\times10^5$ for frictional particles, that too for much deeper layers (40–80 particle diameters).

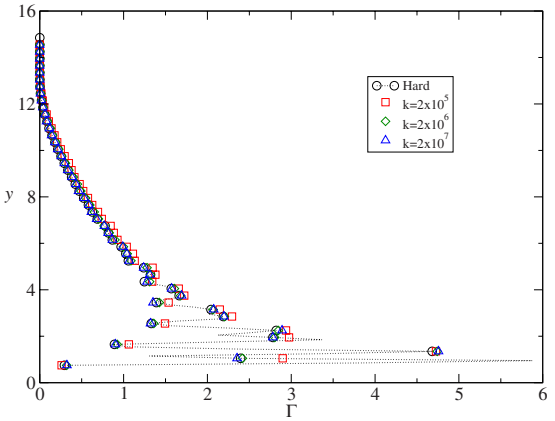

FIG. 9. (Color online) Dissipation profile for hard and soft particle models.

D. Comparison to kinetic theory

We compare the predictions of kinetic theory to numerical results from soft particle simulations for $k=2\times10^6$ and $\theta=14.5°$. The shear stress and pressure obtained from the continuum momentum balance equations [Eqs. (39) and (40)], using the number density profile obtained from the simulations, are compared to simulation results in Fig. 10. There is very good agreement between the two. Figure 11 shows the

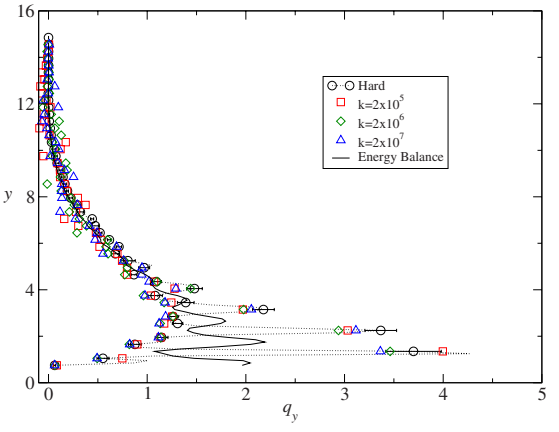

FIG. 11. (Color online) Heat flux in y direction from hard and soft particle simulations. Solid line represents the energy balance estimate from Eq. (41).

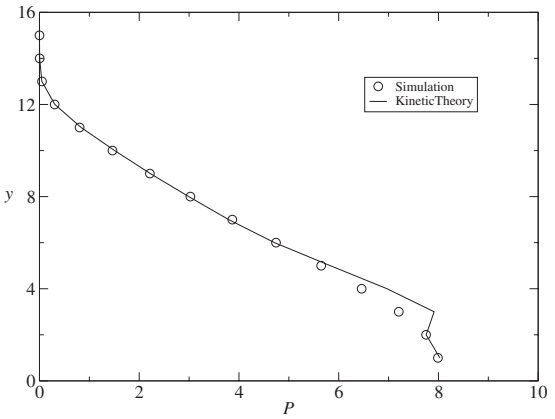

FIG. 12. Pressure profile calculated from simulation (circles) and kinetic theory (line).

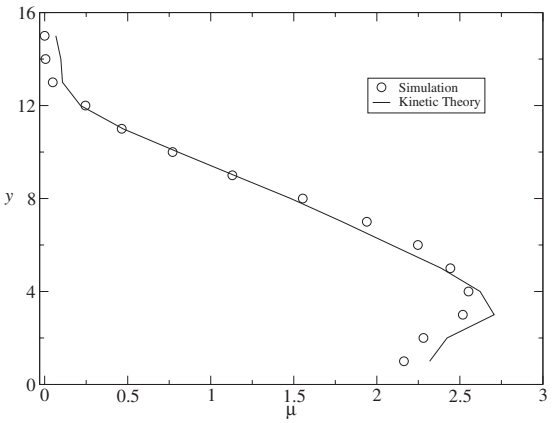

FIG. 14. Comparison of viscosity from simulation (circles) and kinetic theory (line).

comparison between the heat flux profiles obtained from the continuum model [Eq. (41)] to the simulation results. The shear stress, velocity gradient, and dissipation rate from the simulations are used in computing the heat flux from Eq. (41). Again, there is good agreement between the two. The above results indicate the validity of the continuum equations and consistency of the computations since momentum and energy are conserved locally.

Using the values of T and ν from simulation results, we calculate the pressure (P), the dissipation rate (Γ), and the transport coefficients (μ and κ) from constitutive relations using Eqs. (42)–(47) of Jenkins and Richman [34]. An averaging volume with a strip size of $1d$ for T and ν is used in order to obtain smooth profiles. Figures 12 and 13 compare the pressure and dissipation rate from simulation results to kinetic theory predictions. There is very good agreement between the two except slight discrepancy in the region where density $\nu \sim 0.5$. Figure 14 shows a comparison of viscosity from kinetic theory to simulation results. The viscosity is calculated as $\mu = -\tau_{xy}/(dv_x/dy)$ using τ_{xy} and dv_x/dy from simulations and using the kinetic theory expression [Eq. (44)] with T and ν from simulations. Kinetic theory gives good predictions for viscosity over most of the layer.

We compare the heat flux from simulations to that from kinetic theory in Fig. 15. The kinetic theory prediction for heat flux is calculated using Eqs. (45) and (46) with T and ν values taken from simulation results. Figure 15 shows that heat flux predicted from kinetic theory is close to simulation results. A comparison of κ from kinetic theory and simulations has been shown as an inset in Fig. 15. The deviation in κ is due to the error in calculation of temperature gradient which is much smaller than mean velocity gradient.

Figure 16 shows the variation of the mean-square displacement of the particles in y direction with time at different heights from the base. Diffusivity is calculated as the half of the slope of the linear part of the graph. We compare self-diffusion coefficient in y direction (D_{yy}) in Fig. 17 obtained thus from simulation to the kinetic theory prediction using Eq. (48) with appropriate values of a. The theory of Jenkins and Mancini [61] gives good predictions except near the base and at the free surface where as results from Refs. [59,62] predict lower values of the diffusivity. The diffusivity is smaller near the base as compared to the predictions by kinetic theory because the presence of the boundary restricts the diffusion of the particles normal to the surface [63,64]. Deviations near the free surface result from the low number densities and ballistic trajectories.

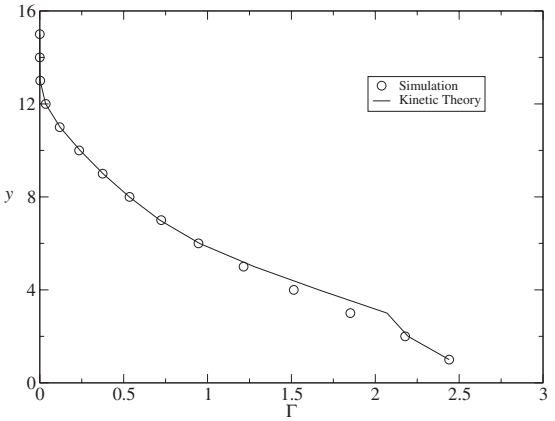

FIG. 13. Dissipation rate calculated from simulation (circles) and kinetic theory (line).

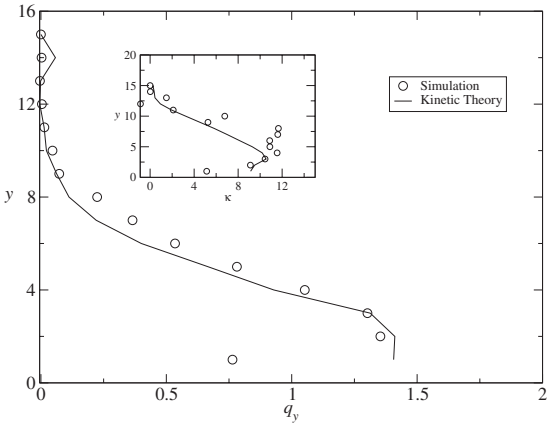

FIG. 15. Comparison of heat flux profiles from simulation (circle) and kinetic theory (line). Inset figure shows the variation of κ with y.

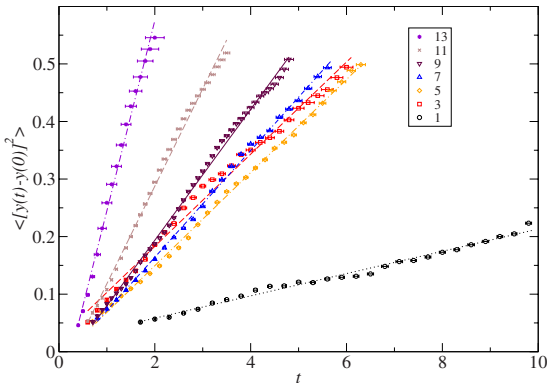

FIG. 16. (Color online) Mean squared displacement of particles in y direction as a function of time (t) for different values of y. Straight lines are the linear fit to the data and the legends represent y, the height from the base. Diffusivity is calculated as half of the slope of the fitted line.

E. Flow of thick layers

We next consider the flow of relatively thick layers. Since hard particle simulations lead to inelastic collapse despite use of TC model, we use only the soft particle model to simulate $H=15d$ and $H=20d$ thick flowing layers. The stiffness in the soft particle model is taken to be $k=2\times10^6$ with $e=0.9$. We report the results at steady state for $\theta=14.5°$ for both cases. Figures 18 and 19 show the velocity, solids fraction, temperature, and stress profiles for $H=15D$ and $H=20D$ thick layers, respectively. A significant slip velocity and a high granular temperature is observed near the base. The temperature decreases with height and varies little in upper part. A dip near the base is observed in solids fraction profile for both cases. The volume fraction of solids, ν, is greater than 0.5 throughout the layer, except near the base and free surface. All these features are similar to $10d$ shallow layer. The density profile for $H=15d$ thick layer shows a small bump near $y=10$ (Fig. 18 top right), which becomes more prominent for $H=20d$ (Fig. 19 top right).

Jenkins [65], in a study of dense flows, used kinetic theory expressions given in Ref. [34] for $\nu<0.49$. For $0.49<\nu<0.6$, he used $G=0.85\nu/(0.64-\nu)$ as given in Ref. [66] and the constitutive expressions are given by Eqs. (42)–(47) in the limit that terms proportional to $1/G$ can be neglected [67]. Garzo and Dufty [68] improved the kinetic theory beyond the assumption of nearly elastic particles extending it to higher values of inelasticities and densities. We omit the expressions given by them and direct the reader to [38,68]. Various quantities of interest are calculated from these kinetic theories, namely, that in Ref. [34] (even for $\nu>0.49$), that in Ref. [65], and Ref. [68] for $\nu>0.49$ (coupled with expressions in Ref. [34] for $\nu<0.49$).

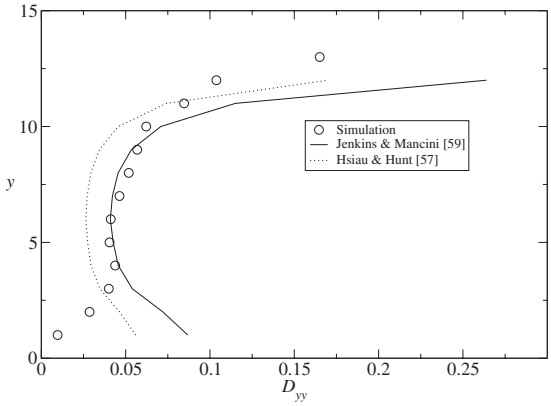

FIG. 17. Comparison of diffusivity measured from simulation (circles) and from kinetic theory [Eq. (48)]. Hsiau and Hunt [59] correspond to $a=8(1+e)$ (dotted line) and Jenkins and Mancini [61] correspond to $a=4\sqrt{6}$ (solid line) in Eq. (48).

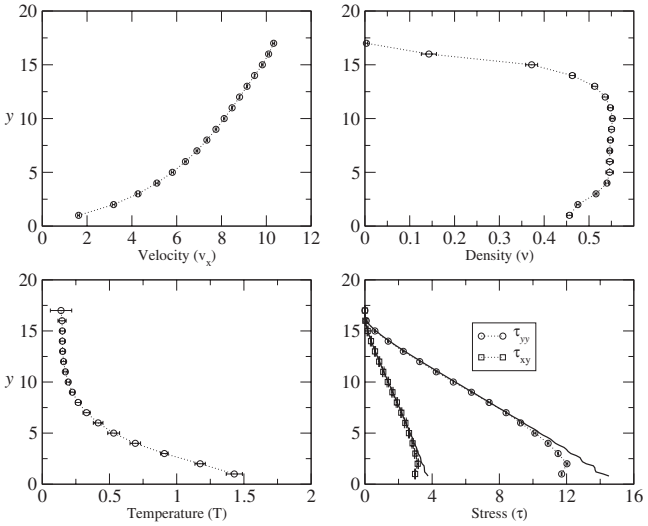

FIG. 18. Velocity, density, temperature, and stress profiles for $H\sim15d$ thick layer. Note that $\nu>0.5$ for most of the part of the layer. Dotted lines are guides to eyes and thick lines represent momentum balance predictions for stresses.

We plot pressure (P), viscosity (η), dissipation (Γ), and heat flux q_y in Figs. 20 and 21. Diffusivity D_{yy} in Fig. 22 is calculated from simulations and from kinetic theories of Jen-

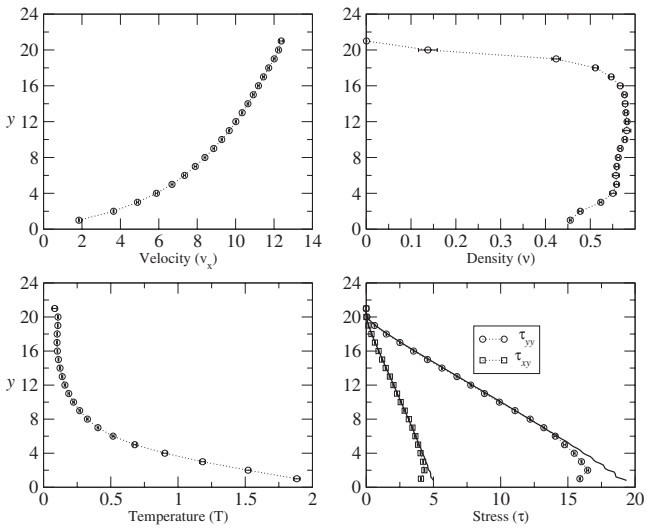

FIG. 19. Velocity, density, temperature, and stress profiles for $H\sim20d$ thick layer. Note that $\nu>0.5$ for most of the parts of the layer. Dotted lines are guides to eyes and thick lines represent momentum balance predictions for stresses.

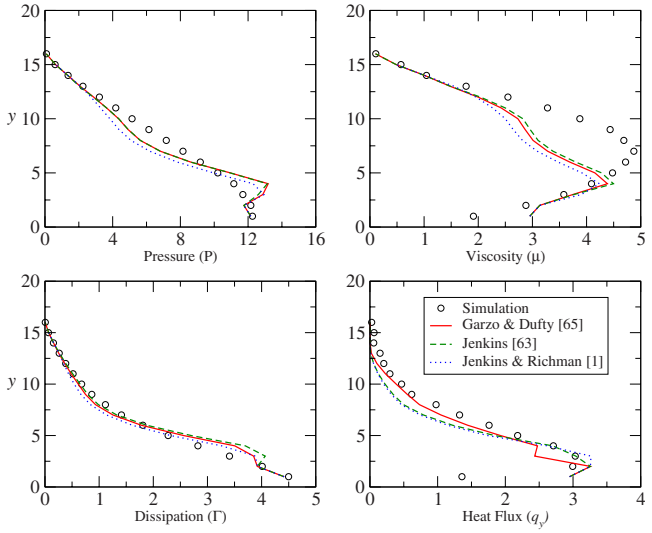

FIG. 20. (Color online) Kinetic theory predictions for pressure, viscosity, dissipation, and heat flux for $H \sim 15d$ thick layer. Symbols are simulation results and lines are kinetic theory predictions.

kins and Mancini [61] and Hsiau and Hunt [59] for both layers. Deviations from kinetic theory prediction are evident and become prominent for higher densities, i.e., for $H = 20D$ (Fig. 21). Contrary to the finding of [38] that kinetic theory overestimates dissipation at high densities, we find that deviations from kinetic theory are small for dissipation even for densities as high as $\nu \approx 0.58$ (Fig. 21, bottom left) and deviations for heat flux (Fig. 21, bottom right) are also not much. The most significant deviations from kinetic theory predictions are observed for pressure (Fig. 21, top left) and shear viscosity (Fig. 21, top right). Large deviations in pressure and viscosity in the middle region of the layer are obtained due to the sharp decrease in the density near $y = 10$ (Fig. 19, top right).

Mitarai and Nakanishi [38] reported that both normal stress and dissipation are consistently overestimated by ki-

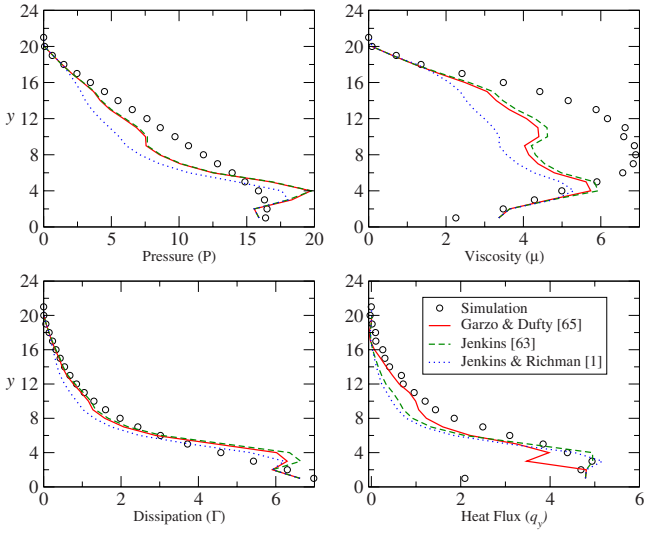

FIG. 21. (Color online) Kinetic theory predictions for pressure, viscosity, dissipation, and heat flux for $H \sim 20d$ thick layer. Symbols are simulation results and lines are kinetic theory predictions.

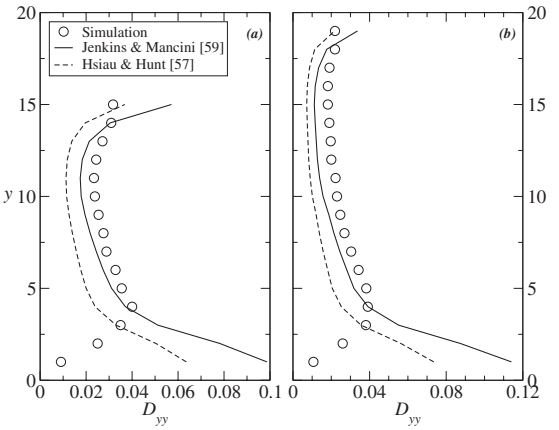

FIG. 22. Diffusivity D_{yy} for (a) $H=15d$ and (b) $H=20d$ thick layers. Symbols are simulation results and lines are predictions from kinetic theory.

netic theory for higher densities. However, we find that the deviation from kinetic theory is not monotonic and kinetic theory overestimates the pressure and dissipation only in a small portion of the lower part of the layer. Though the predictions of the shear stress (and hence viscosity) from kinetic theory are very good up to $\nu=0.58$ for particles with $e=0.92$ in case of homogeneous shear (Ref. [38]), present study of inhomogeneous shear flow of particles with $e=0.9$, however, shows significant difference for viscosity calculated from simulations and that predicted by kinetic theory. Note that even in Ref. [38], substantial deviation is observed for $e=0.7$ as well as $e=0.98$. The authors suggest that the excellent match for $e=0.92$ is accidental and conclude that shear stress has a complicated dependence on e. The computed diffusivity, D_{yy}, is shown in Fig. 22 for the two cases. The kinetic theory underpredicts the diffusivity in both cases.

VI. CONCLUSION

We studied the flow of smooth, slightly inelastic ($e=0.9$) spheres down a bumpy inclined surface using both hard and soft particle models. The TC model [19] was used to prevent inelastic collapse for the hard particle simulation of shallow layers. Steady-state flow was obtained for a narrow range of angles ($13° - 14.5°$) as compared to frictional particles ($23° - 28.5°$) [7]. The profiles for the mean velocity, density, granular temperature, components of stress tensor, dissipation, and granular heat flux vector were obtained at steady state. Macroscopic profiles of all the quantities of interest for the hard particles and soft particles were found to be identical for the stiffness, $\bar{k} \geq 2 \times 10^6$. This value is larger than the value typically used ($\bar{k}=2 \times 10^5$) in soft particle simulations of frictional particles. Apart from the macroscopically identical picture of hard and soft particle simulations for sufficiently high stiffness, we found that at microscopic level too, the interaction of soft particles with high stiffness tends to approach hard-particle-type binary collisions and the number of contacts at an instant vary as $N_c \sim \bar{k}^{-1/2}$.

We derived expressions for calculation of the dissipation and contact granular heat flux associated with the granular temperature for both soft and hard particle models using a theoretical approach. Since the nature of particle-particle interaction is quite different for the hard and soft particles, the expressions for the contact heat flux are quite different. The excellent agreement between the heat flux profiles of hard and soft particles and that from energy balance validates the proposed expressions. The expressions for the contact stress tensor are also derived using the approach and are identical to those reported earlier.

The simulation results for $\bar{P}$, $\bar{\tau}_{xy}$, and $\bar{q}_y$ are shown to match continuum momentum and energy balance predictions indicating the consistency of the results and establishing the validity of the continuum approach for even shallow granular flows. Using simulation results for $\bar{T}$ and ν, the dissipation due to inelastic collisions ($\bar{\Gamma}$), pressure ($\bar{P}$), viscosity ($\bar{\mu}$), and heat flux ($\bar{q}_y$) are computed using the constitutive equations of the [34] theory for smooth inelastic spheres and compared to simulation results. The agreement between theory and simulations for $\bar{\Gamma}$, $\bar{P}$, $\bar{\mu}$, and $\bar{q}_y$ is found to be very good for the $10d$-thick layer. This is surprising considering the extent of layering in the system. However, kinetic theory predictions start deviating from simulation results at higher densities for thick layers with the most significant deviation being observed for pressure and shear viscosity. Dissipation, contrary to the results reported earlier in literature, is quite well predicted.

The system studied has the important features of typical terrestrial flows—shallow flowing depths, high volume fractions, and layering—although the particles are frictionless. The results provide guidance for the choice of an important parameter for soft particle simulations—the stiffness. They also indicate the range of validity of the continuum balance equations and constitutive equations from kinetic theory.

[1] E. Azanza, F. Chevoir, and P. Moucheront, J. Fluid Mech. **400**, 199 (1999).
[2] C. Ancey, Phys. Rev. E **65**, 011304 (2001).
[3] O. Pouliquen, Phys. Fluids **15**, 1588 (1999).
[4] S. B. Savage, J. Fluid Mech. **92**, 53 (1979).
[5] C. S. Campbell and C. E. Brennen, Trans. ASME **52**, 171 (1985).
[6] O. R. Walton, Mech. Mater. **16**, 239 (1993).
[7] L. E. Silbert, D. Ertas, G. S. Grest, T. C. Halsey, D. Levine, and S. J. Plimpton, Phys. Rev. E **64**, 051302 (2001).
[8] D. Ertaş, G. S. Grest, T. C. Halsey, D. Levine, and L. E. Silbert, Europhys. Lett. **56**, 214 (2001).
[9] W. Bi, R. Delannay, P. Richard, N. Taberlet, and A. Valance, J. Phys.: Condens. Matter **17**, S2457 (2005).
[10] S. Dippel and D. Wolf, Comput. Phys. Commun. **121-122**, 284 (1999).
[11] R. Delannay, M. Louge, P. Richard, N. Taberlet, and A. Valance, Nature Mater. **6**, 99 (2007).
[12] N. Taberlet, P. Richard, and R. Delannay, Comput. Math. Appl. **55**, 230 (2008).
[13] L. E. Silbert, J. W. Landry, and G. S. Grest, Phys. Fluids **15**, 1 (2003).
[14] T. Poschel, J. Phys. II **3**, 27 (1993).
[15] X. M. Zheng and J. M. Hill, Powder Technol. **86**, 219 (1996).
[16] X. M. Zheng and J. M. Hill, Comput. Mech. **22**, 160 (1998).
[17] L. E. Silbert, G. S. Grest, and S. J. Plimpton, Phys. Fluids **14**, 2637 (2002).
[18] L. E. Silbert, D. Ertas, G. S. Grest, T. C. Halsey, and D. Levine, Phys. Rev. E **65**, 051307 (2002).
[19] S. Luding and S. McNamara, Granular Matter **1**, 113 (1998).
[20] R. Brewster, L. E. Silbert, G. S. Grest, and A. J. Levine, Phys. Rev. E **77**, 061302 (2008).
[21] J. Duran, *Sands, Powders, and Grains: An Introduction to the Physics of Granular Materials* (Springer-Verlag, New York, 2000).
[22] S. Luding, E. Clement, A. Blumen, J. Rajchenbach, and J. Duran, Phys. Rev. E **50**, 4113 (1994).
[23] J. T. Jenkins and S. B. Savage, J. Fluid Mech. **130**, 187 (1983).
[24] C. K. K. Lun, S. B. Savage, D. J. Jefferey, and N. Chepurniy, J. Fluid Mech. **140**, 223 (1984).
[25] N. Mitarai and H. Nakanishi, Phys. Rev. E **67**, 021301 (2003).
[26] W. R. Ketterhagen, J. S. Curtis, and C. R. Wassgren, Phys. Rev. E **71**, 061307 (2005).
[27] L. E. Silbert, G. S. Grest, R. Brewster, and A. J. Levine, Phys. Rev. Lett. **99**, 068002 (2007).
[28] K. A. Reddy and V. Kumaran, Phys. Rev. E **76**, 061305 (2007).
[29] S. Klongboonjit and C. S. Campbell, Phys. Fluids **20**, 103301 (2008).
[30] R. D. Wildman, T. W. Martin, P. E. Krouskop, J. Talbot, J. M. Huntley, and D. J. Parker, Phys. Rev. E **71**, 061301 (2005).
[31] C. Bizon, M. D. Shattuck, J. B. Swift, and H. L. Swinney, Phys. Rev. E **60**, 4340 (1999).
[32] M. Y. Louge, Phys. Fluids **6**, 2253 (1994).
[33] N. Mitarai and H. Nakanishi, Phys. Rev. Lett. **94**, 128001 (2005).
[34] J. T. Jenkins and M. W. Richman, Arch. Ration. Mech. Anal. **87**, 355 (1985).
[35] C. K. K. Lun, J. Fluid Mech. **233**, 539 (1991).
[36] J. T. Jenkins and C. Zhang, Phys. Fluids **14**, 1228 (2002).
[37] D. K. Yoon and J. T. Jenkins, Phys. Fluids **17**, 083301 (2005).
[38] N. Mitarai and H. Nakanishi, Phys. Rev. E **75**, 031305 (2007).
[39] J. M. Montanero, V. Garzo, A. Santos, and J. J. Brey, J. Fluid Mech. **389**, 391 (1999).
[40] A. Santos, J. M. Montanero, J. W. Dufty, and J. J. Brey, Phys. Rev. E **57**, 1644 (1998).
[41] S. B. Savage and R. Dai, Mech. Mater. **16**, 225 (1993).
[42] M. Babic, Phys. Fluids **9**, 2486 (1997).
[43] M. Y. Louge, J. T. Jenknis, and M. A. Hopkins, Phys. Fluids A **2**, 1042 (1990).
[44] C. S. Chou, Proc. Natl. Sci. Counc., Repub. China, Part A: Phys. Sci. Eng. **24**, 317 (2000).
[45] M. Babić, ASME J. Appl. Mech. **60**, 59 (1993).
[46] Y. Lan and A. Rosato, Phys. Fluids **7**, 1818 (1995).

[47] M. D. Shattuck, C. Bizon, J. B. Swift, and H. L. Swinney, Physica A **274**, 158 (1999).
[48] O. Herbst, P. Muller, and A. Zippelius, Phys. Rev. E **72**, 041303 (2005).
[49] R. Soto, Phys. Rev. E **69**, 061305 (2004).
[50] Simulation of moderately thick layers $h \approx 20d$ caused collapse near the base despite using TC model with most of the collisions being forced to be nondissipative.
[51] J. P. Tignol, *Galois' Theory of Algebraic Equations* (World Scientific, Singapore, 2001).
[52] L. E. Dickson, *Elementary Theory of Equations* (Wiley, New York, 1914).
[53] S. Luding, E. Clement, A. Blumen, J. Rajchenbach, and J. Duran, Phys. Rev. E **49**, 1634 (1994).
[54] P. Deltour and J. L. Barrat, J. Phys. I **7**, 137 (1997).
[55] D. Goldman, M. D. Shattuck, C. Bizon, W. D. McCormick, J. B. Swift, and H. L. Swinney, Phys. Rev. E **57**, 4831 (1998).
[56] We have also used velocity Verlet algorithm to integrate Eqs. (6) and (7) and found that the results are identical using both integration schemes.
[57] C. S. Campbell and A. Gong, J. Fluid Mech. **164**, 107 (1986).
[58] C. S. Campbell, J. Fluid Mech. **203**, 449 (1989).
[59] S. S. Hsiau and M. L. Hunt, ASME J. Heat Transfer **115**, 541 (1993).
[60] A. D. Rosato, Y. Lan, and M. W. Richman, Powder Technol. **182**, 228 (2008).
[61] J. T. Jenkins and F. Mancini, ASME J. Appl. Mech. **54**, 27 (1987).
[62] D. V. Khakhar, J. J. McCarthy, and J. M. Ottino, Chaos **9**, 594 (1999).
[63] E. R. Dufresne, T. M. Squires, M. P. Brenner, and D. G. Grier, Phys. Rev. Lett. **85**, 3317 (2000).
[64] B. Lin, J. Yu, and S. A. Rice, Phys. Rev. E **62**, 3909 (2000).
[65] J. T. Jenkins, Granular Matter **10**, 47 (2007).
[66] S. Torquato, Phys. Rev. E **51**, 3170 (1995).
[67] Jenkins [65] accounts for a chain length L of particles instead of d in Eq. (47). Since using this chain length enhances the discrepancy from simulation results, we use $L=d$.
[68] V. Garzó and J. W. Dufty, Phys. Rev. E **59**, 5895 (1999).